Ultrafast dynamics in 2D materials and heterostructures visualized with time- and angle-resolved photoemission

Thomas K. Allison[a], Zachary H. Withers[a], Ziling Li[b], Jin Bakalis[a], Sergii Chernov[a], Shuyu Cheng[b], Gerd Schönhense[c], Xu Du[a], Roland Kawakami[b], and Alice Kunin[d]

[a]Stony Brook University, Stony Brook, NY 11790, USA
[b]The Ohio State University, Columbus, OH 43210, USA
[c]Johannes Gutenberg-Universität, Mainz, Germany
[d]Princeton University, Princeton, NJ 08544, USA

ABSTRACT

The optical and electronic properties of two-dimensional (2D) materials make them attractive for a variety of applications in quantum information processing, solar-energy harvesting, and catalysis. However, the dynamics of electrons, holes, and excitons formed after photo-excitation are often complex and involve many states that are optically dark, making their characterization with optical spectroscopy alone difficult. We present our recent work imaging the quantum states of 2D materials and their heterostructures in momentum space using time- and angle-resolved photoemission. A unique combination of tunable ultrashort extreme ultraviolet (XUV) pulses with 61 MHz repetition rate and time-of-flight momentum microscopy (ToF k-mic) enables the parallel recording of electron dynamics in all states across the full Brillouin zone after perturbative excitation. We will present results on pseudospin dynamics in graphene, valley circular dichroism in monolayer WS_2, and hybridized excitons in $MoSe_2/WS_2$ bilayers.

Keywords: Photoelectron spectroscopy, high-order harmonic generation, frequency combs, momentum microscopy.

1. INTRODUCTION

The language of condensed-matter physics and quantum materials lives in momentum space, both conceptually and in computational methods. Even for complex highly-correlated systems that are not described well with one-particle pictures, we formulate the problem and the relevant interactions in a momentum-space basis using each participating quasiparticle's energy, momentum, and spin as quantum numbers.

Spectroscopy using ultrashort laser pulses can track dynamics after excitation with light, and in principle this can be used to dissect the complex interactions between spin, lattice, charge, and valley degrees of freedom in quantum materials.[1] However, unfortunately most ultrafast spectroscopy observables involve drastic integrations over momentum and spin which reduces their information content and obscures their meaning. Most ultrafast spectroscopy methods are also blind to "dark states" that cannot be probed due to selection rules.

For characterizing ground states of quantum materials, angle-resolved photoelectron spectroscopy (ARPES) has emerged as the premier method for momentum-space measurements, and is sometimes called the "gold standard" for measuring electronic structure. From a clean surface, the photoemission process preserves an electron's momentum parallel to the surface, $k_{\|}$, such that measuring the angle a photoelectron is emitted from the surface and its kinetic energy directly reports on the electron's energy and momentum in the solid. More formally, ARPES measurements give the one-particle spectral function, which reduces to the band structure $\varepsilon(\mathbf{k})$ in the absence of strong interactions.[2]

The extension of ARPES to the time domain using pump/probe methods with ultrashort pulses then seems quite natural and obvious: To understand non-trivial excited states or complicated dynamics initiated by optical

Further author information: (Send correspondence to T.K.A. or A.K.)
T.K.A. E-mail: thomas.allison@stonybrook.edu
A.K. E-mail: kunin@princeton.edu

excitation, use the "gold standard" observable. However, the implementation of time-resolved ARPES (tr-ARPES) has always been very challenging. The fundamental issue at the root of all difficulties is data rate. Adding pump pulses to the ARPES experiment adds 4 dimensions to the data set, namely pump-probe delay, pump wavelength, pump fluence, and pump polarization. Furthermore, the signal size in an excited-state ARPES measurement is inherently much smaller than in ground-state measurements, since only a fraction of the sample's electrons are excited by the pump pulse. Together, these factors create a severe data-rate challenge for tr-ARPES experiments, and this severe data rate problem has forced practitioners of tr-ARPES to make correspondingly severe compromises in order to perform experiments. For example, the highest performing tr-ARPES setups in terms of sensitivity and resolution achieve this using probe pulses with 6 eV photon energy,[3,4] which are easier to produce than the extreme-ultraviolet (XUV) photons used at synchrotrons and produce less secondary electrons, but also only give access to just a tiny fraction of the Brillouin zone near Γ.

The data rate in a time-resolved ARPES experiment can be expressed using the simple formula

$$\text{Data Rate} \propto (\text{repetition rate}) \times (e^- \text{ collection efficiency}) \times (\text{pump fluence}) \times (\text{probe fluence}) \tag{1}$$

The physics of the sample dynamics and XUV photoemisson present intrinsic limitations on the last two factors. The probe fluence, or number of XUV photons per pulse that can be applied to the sample, is limited by the so-called vacuum space charge effect, wherein the mutual repulsion of photoelectrons created at the surface can cause severe broadening, shifts, and other distortions of the photoelectron spectrum.[5–7] * The pump fluence is dictated by the sample physics under study. To study laser-induced phase transitions, for example ultrafast demagnetization[12] or structural phase transitions,[13] strong pump fluences in the mJ/cm^2 regime can be used, which produces large and easily discernible changes in the sample's electronic structure. In contrast, to study the intrinsic quasi-particle dynamics of optically excited electrons, holes, and/or excitons as might occur in optoelectronic devices, excitation fluences must be in the $\sim\mu$J/cm^2 regime or smaller,[1,14] giving signal sizes orders of magintude lower. Indeed, for this reason, most tr-ARPES studies using XUV photons have been restricted to studying strongly excited samples until recently.

The experimentalist has more control over the first two factors of repetition rate and electron collection efficiency, and recently large gains have been achieved on both. High repetition rate ultrashort XUV pulses suitable for tr-ARPES can be achieved using high harmonic generation (HHG) of femtosecond pulse trains with high average power. HHG sources for ARPES with repetition rates $\gtrsim$1 MHz have been achieved either using high-power Yb-based laser systems and "single-pass" HHG with tight focusing[15–18] or the technique of cavity-enhanced high harmonic generation (CE-HHG),[5,19] in which harmonics are produced in a resonant enhancement cavity.[20,21] Single-pass systems can operate with commercial lasers and also commercial optical parametric amplifiers for generating tunable pump pulses. CE-HHG offers higher repetition rates and photon energies, and can be accomplished with a laser with lower average power and thus less cost, however it requires expertise in frequency combs and laser stabilization, and creating tunable pump pulses is less straightforward. Given these subtleties, practitioners in the field continue to develop new instruments using both approaches.

In contrast to the different approaches taken for MHz HHG light sources, most high-performance tr-ARPES systems have now adopted time-of-flight momentum microscopy (ToF k-mic)[22,23] for the photoelectron analyzer. ToF k-mic provides full 2π collection efficiency and detection of the full (k_x, k_y, E) data cube in parallel. Furthermore, by inserting an aperture in a real-space image plane of the microscope, photoelectron signals from a micron-sized region of interest (ROI) on the sample surface can be selected, enabling micro-ARPES even with large XUV spot sizes.

Over the past 10 years, at Stony Brook we have developed a unique beamline for high-performance tr-ARPES measurements combining cavity-enhanced HHG and ToF k-mic, with data rates more than 4 orders of magnitude larger than what could be achieved just a few years ago. With this instrument, informative ground-state photoemission signals covering the full Brillouin zone can now be acquired in seconds and pump-probe

*The space charge constraints are particularly acute using the new generation of photoelectron analyzers based on momentum microscopy, restricting photoemission to just 10s of electrons per pulse at the sample for high resolution work,[8–10] although this can be improved somewhat for experiments using high-energy photons in the x-ray regime with new analyzer front lens configurations.[11]

experiments in the pertubative excitation regime in just a few minutes. This high data rate enables performing experiments under a wide range of conditions to explore the large parameter space of pump/probe ARPES on non-trivial systems, as exemplified by ref. 24, where we reported the first momentum-space observations of valley circular dichroism in a monolayer material in a series of systematic pump/probe measurements, all taken in the perturbative excitation limit with pump fluences < 10 $\mu J/cm^2$, even from an exfoliated flake only 10 microns in size!

In this article we describe this unique instrumentation and give several exampes of measurements in 2D materials produced by exfoliation. Section 2 gives an overview of the Stony Brook ARPES beamline, including the endstation and time-of-flight momentum microscope. Section 3 describes momentum-space measurements of valley circular dichroism in monolayer WS_2. Section 4 describes momentum-space visualization of pseudospin selection rules in monolayer graphene, and section 5 describes experiments in transition-metal dichalcogenide (TMD) heterostructures.

2. THE STONY BROOK TIME-RESOLVED ARPES BEAMLINE

The Stony Brook tr-ARPES beamline is shown in figure 1. An 80 W, 155 fs frequency comb laser[25] with a repetition rate of 61 MHz and a center wavelength of 1.035 μm ($h\nu = 1.2$ eV) is passively amplified in a six-mirror enhancement cavity with a 1% transmission input coupler. Typical intracavity powers for generating harmonics range from 5-11 kW, depending on the generating gas and desired harmonic spectrum. We lock the laser to the cavity using a two-point Pound-Drever-Hall lock as described in refs. 26,27. Harmonics are generated at an intracavity focus and reflected from a sapphire wafer placed at Brewster's angle for the resonant 1.035 μm light. When generating harmonics, we flow a mix of ozone and O_2 from a commercial ozone generator on each intracavity optic to prevent hydrocarbon contamination, allowing continuous operation.

The outcoupled harmonics are collimated by an $f = 350$ mm toroidal mirror at 3 degrees grazing angle (TM1) that forms the first part of a pulse-preserving monochromator similar to the design of Frassetto et al.[28] The harmonics then strike a motorized grating at a 4 degree grazing angle and are refocused by a second $f = 350$ mm toroidal mirror (TM2) at an adjustable slit. The exit slit plane of the monochromator is 1:1 imaged to the sample using another 350 mm focal length toroid at 3 degrees grazing angle (TM3). Photoelectrons from the sample are imaged to a delay-line detector (DLD) using a custom time-of-flight momentum microscope with

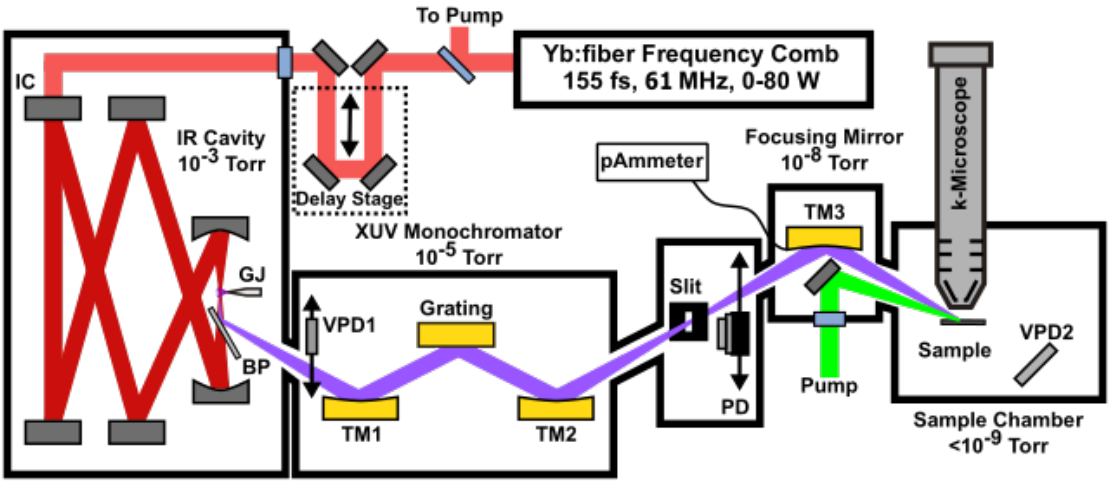

Figure 1. **The Stony Brook tr-ARPES beamline.** High-order harmonics are generated in a gas jet (GJ) at the focus of a six-mirror enhancement cavity and reflected out of the cavity using a sapphire plate at Brewster's angle (BP). A pulse-preserving monochromator consisting of two toroidal mirrors (TM1 and TM2), an off-plane diffraction grating, and an exit slit, selects a single harmonic for delivery to a sample at the focus of time-of-flight momentum microscope. More details in the text.

adjustable apertures at both real-space and momentum-space image planes for selecting regions of interest to pass to the detector in both real and momentum space.

We routinely attain a flux of $\sim 1 \times 10^{11}$ photons/second delivered to the sample in a single harmonic and spot sizes less than 30 μm. This flux produces $> 10^9$ photoelectrons/second (500 pA) at the sample, or 10s of electrons per pulse. Under these conditions, broadening of the photoelectron spectra due to space charge is less than 50 meV.[9] We use two grids in front of the DLD to prevent low-energy electrons (mostly secondaries) from reaching the detector, reducing the count rate at the detector to less than 10^6 electrons per second for electrons near or above the Fermi level. Including ToF resolution, voltage fluctuations, and dispersion of the high-pass filter, we have obtained an overall resolution of 100 meV.[9] The time resolution, measured via cross-correlation of pump and probe pulses using fast-relaxing tr-ARPES signals, is 200 fs FWHM.

3. VALLEY CIRCULAR DICHROISM IN MONOLAYER WS_2

The discovery of valley-selective circular dichroism in monolayer TMDs[29–36] has sparked enormous interest in these materials as platforms for novel optoelectronic devices. Right (σ^+) and left (σ^-) circularly polarized light selectively excites interband transitions in the inequivalent K^+ and K^- valleys, respectively, where the band extrema are located.[37,38] Strong Coulomb forces and spin-orbit coupling in these materials yield tightly bound exciton states of definite spin character, with the potential for long-lived, spin-valley locked excitons.[39–44] Many optical spectroscopy techniques have been employed to investigate valley lifetimes and depolarization mechanisms in monolayer TMDs, including photoluminescence,[33,45–48] differential transmission,[49,50] time-resolved Kerr and Faraday rotation,[51–58] and multidimensional spectroscopies,[59–63] among others.[64] Valley polarization lifetimes ranging from a few picoseconds[46,47,50] to hundreds[49,52,54] or tens[62] of femtoseconds have been reported, depending on the system under study and the spectroscopy method. Interpreting this body of work has been the subject of considerable debate.[50,62,65–68] In particular, it has been debated whether the dominant mechanism of valley depolarization is due to the direct or exchange terms of the Coulomb-interaction Hamiltonian that couples excitons in different valleys.[50,59,68–78]

We set out to resolve this debate with momentum-resolved measurements as illustrated in figure 2a). Pump pulses with $h\nu = 2.4$ eV and variable polarization illuminate an exfoliated monolayer WS_2 sample followed by p-polarized probe pulses with $h\nu = 25.2$ eV. The monolayer WS_2 sample is isolated from the silicon substrate via a ∼10 nm thick hexagonal boron nitride (hBN) layer. Figure 2b) shows the raw momentum-space signal, with signals in the K^+ and K^- valleys recorded in parallel using the ToF k-mic. Figure 2c) shows time-resolved traces of the signals in the K^+ and K^- valleys after excitation with σ^+-polarized light. We observed rapid depolarization within 50 fs. Furthermore, comparing the energy and momentum distributions in the K^+ and

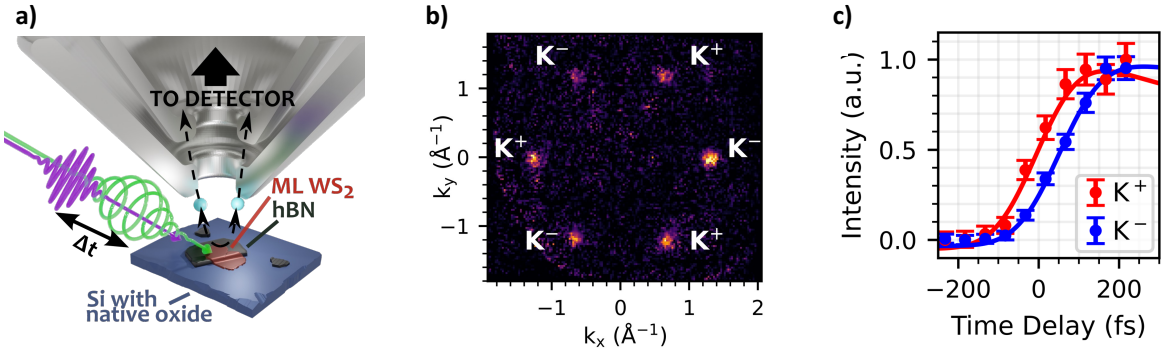

Figure 2. **Monolayer WS_2 results.** a) Experimental setup. A monolayer WS_2 sample supported on ∼10 nm thick hBN is illuminated by 517 nm pump pulses with variable polarization (green) and p-polarized XUV pulses. Photoelectrons are collected with the time-of-fight momentum microscope (gray). b) Raw momentum-space exciton signals after photoexcitation. c) Valley-resolved signal vs. pump/probe delay recorded with circularly polarized light. The σ^+ polarization preferentially excites the K^+ valleys, but excitons rapidly depolarize within 50 fs. Figure is adapted from ref. 24, where more data and detailed analysis can be found.

K^- valleys, we observe conservation of energy and momentum in the valley depolarization process,[24] consistent with the intervalley Coulomb-exchange driven depolarization mechanism and inconsistent with depolarization driven by the Coulomb-direct interaction.

4. PSEUDOSPIN DYNAMICS IN GRAPHENE

The first 2D material realized was graphene, and monolayer and few-layer graphene still play a major role in 2D materials research. In optoelectronics, the broadband absorption and ultrafast relaxation of excited electrons in graphene make it an ideal material for saturable absorbers in mode-locked lasers,[79] and the long spin lifetime make it attractive for spintronic devices.[80]

Graphene presents an additional quantum number called pseudospin. The pseudospin ϕ refers to the relative phase of the Bloch wavefunction on the two equivalent carbon sublattices A and B in its honeycomb lattice via $\psi = \psi_A + e^{i\phi}\psi_B$. It also corresponds to the angular position of Bloch states around the K points in the Brillouin zone, as illustrated in figure 3b). Photoexcitation of electrons from the valence band to the conduction band creates pseudospin polarization via the **k**-dependence (and thus ϕ-dependence) of the optical matrix elements.[81] This phenomena has been previously studied using optical spectroscopy[82–84] and also using tr-ARPES.[85,86] However, the previous tr-ARPES studies were carried out on either graphite or heavily doped graphene, such that there is a large occupied density of states at the Fermi level, and also with very high excitation fluence, such that all observed dynamics and distributions are dominated by rapid electron-electron scattering/thermalization and pseudospin anisotropy is rapidly lost. In contrast, at lower excitation fluence in neutral graphene, complete thermalization of the electrons is slowed and a non-thermal pseudospin-polarized distribution is expected to persist longer.[87]

In our measurements with a fluence of only 45 μJ/cm^2, and in neutral (i.e., undoped) graphene, we observe a nonthermal distribution of electrons that persists within our 200 fs instrument response time. Figure 3 shows momentum distributions of pseudospin-polarized electrons around one of the K points excited by 2.4 eV photons polarized in either the x or y direction, along with simulations of the signal using band structure and matrix elements for both pump and probe steps of the experiment derived from tight binding theory.[81,88] Inclusion of the **k**-dependence of the probe photoemission matrix element is essential in modeling the signals. Overall excellent agreement is seen between our experiment and this simple theory, indicating the nascent excited distribution

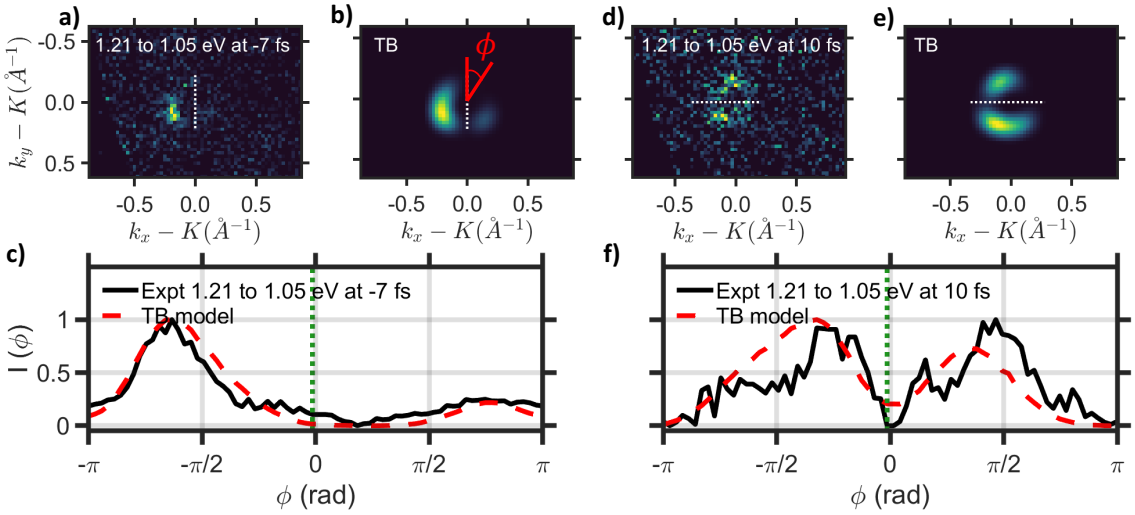

Figure 3. **Pseudospin polarization in graphene.** a) Raw experimental momentum-space image of electrons around a graphene K point between 1.05 and 1.21 eV above the Fermi level after excitation with 2.4 eV photons polarized in the y direction. b) Simulation of the signal using band structures and matrix elements. c) Comparison of the angle-dependent signals between theory and experiment. d)-f) Same as a)-c) except for x-polarized excitation.

at $\varepsilon = h\nu/2$ above the Fermi level persists for a substantial fraction of our instrument response time. Further analysis of this data including the energy- and fluence-dependence of the anisotropy will appear in a forthcoming publication.[89]

5. EXCITON STATES IN TWISTED HETEROSTRUCTURES

Vertically stacking heterobilayers of TMDs with a finite twist angle leads to the emergence of new, tunable excitonic properties due to the moiré superlattice that is formed. $MoSe_2/WS_2$ heterobilayers present a special case among TMD heterobilayers as the conduction band alignment of the two layers is nearly degenerate, leading to hybridization between intralayer and spatially-indirect interlayer excitons. Optical measurements have shown emerging angle- and temperature-dependent features in $MoSe_2/WS_2$ structures proposed to correspond to the formation of hybridized excitons,[90,91] but these momentum-integrated measurements do not allow for the direct observation of electron sharing between the two layers.

While small twist angles θ and $60° - \theta$ are expected to lead to strong hybridization due to the overlap of K_{MoSe_2} and K_{WS_2} in momentum space, larger angles exhibit weaker or absent spectral signatures of hybridization.[91] However, recent work has suggested that near 40° twist angle should exhibit a revival of hybridization due to the moiré reciprocal lattice wavevector becoming commensurate with the momentum mismatch of K_{MoSe_2} and K'_{WS_2}.[90]

The electron sharing between the two layers (or lack thereof) and the dynamics of exciton formation can be directly visualized with our high-performance tr-ARPES instrument. Figure 4 shows exciton signals in $MoSe_2/WS_2$ heterobilayers at twist angles of a) 40.2 ± 0.9° and b) 58.0 ± 0.3° at 90 K. In 40.2° twisted $MoSe_2/WS_2$, our measurements resolve the occupation of both of the monolayer Brillouin zones up to few ps timescales. The dynamics suggest that intralayer $MoSe_2$ excitons rather than hybridized excitons ultimately persist at longer timescales. In the 58.0° twisted heterobilayer, we observe the prominent formation of higher energy $K - Q$ dark excitons in the interior of the Brillouin zone.

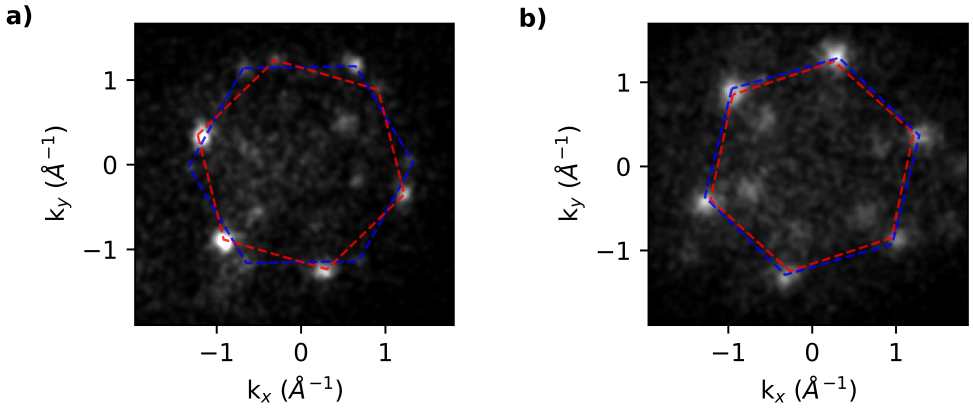

Figure 4. **$MoSe_2/WS_2$ bilayer results.** Exciton signal measured at 90K for $MoSe_2/WS_2$ twisted heterobilayers at twist angles of a) 40.2° ($h\nu_{probe} = 27.6$ eV) and b) 58.0° ($h\nu_{probe} = 25.2$ eV). Red (blue) dashed lines indicate the $MoSe_2$ (WS_2) Brillouin zone.

6. CONCLUSION

The combination of MHz-repetition rate fs XUV pulses from HHG and ToF k-mic enables tr-ARPES measurements that are qualitatively different than what was possible just a few years ago. The two main qualitative differences are 1) tr-ARPES experiments can now be performed with excitation fluences in the few $\mu J/cm^2$ regime, such that the intrinsic quasi-particle dynamics of materials after perturbative excitation can now be studied, and 2) tr-ARPES experiments can now be performed on micron-sized samples, such as those produced via exfoliation, dramatically expanding the types of materials that can be studied. We have illustrated what

can be done in this qualitatively new regime here with our results on bound excitons in monolayers and bilayers and there is additionally much work from other research groups in this area as well.[16,92–94] Together, this work represents a new paradigm in ultrafast spectroscopy, wherein electronic wave functions and electronic motion are directly visualized in momentum space.

7. ACKNOWLEDGEMENTS

This material is primarily based upon work supported by the U.S. Department of Energy, Office of Science, Office of Basic Energy Sciences under Award No. DE-SC0022004 and the Air Force Office of Scientific Research under FA9550-20-1-0259. R. K. K. acknowledges support from the U.S. National Science Foundation under Grant No. CHE-1935885. X. D. acknowledges support from the U.S. National Science Foundation under Grant No. DMR1808491. Z. H. W. acknowledges support from the U.S. National Science Foundation Graduate Research Fellowship Program.

REFERENCES

[1] Basov, D. N., Averitt, R. D., van der Marel, D., Dressel, M., and Haule, K., "Electrodynamics of correlated electron materials," *Rev. Mod. Phys.* **83**, 471–541 (Jun 2011).

[2] Sobota, J. A., He, Y., and Shen, Z.-X., "Angle-resolved photoemission studies of quantum materials," *Rev. Mod. Phys.* **93**, 025006 (May 2021).

[3] Smallwood, C. L., Kaindl, R. A., and Lanzara, A., "Ultrafast Angle-Resolved Photoemission Spectroscopy of Quantum Materials," *EPL* **115**(2), 27001 (2016).

[4] Koralek, J. D., Douglas, J. F., Plumb, N. C., Griffith, J. D., Cundiff, S. T., Kapteyn, H. C., Murnane, M. M., and Dessau, D. S., "Experimental setup for low-energy laser based angle resolved photoemission spectroscopy," *Review of Scientific Instruments* **78**, 053905 (2007).

[5] Corder, C., Zhao, P., Bakalis, J., Li, X., Kershis, M. D., Muraca, A. R., White, M. G., and Allison, T. K., "Ultrafast extreme ultraviolet photoemission without space charge," *Structural Dynamics* **5**(5), 054301 (2018).

[6] Plotzing, M., Adam, R., Weier, C., Plucinski, L., Eich, S., Emmerich, S., Rollinger, M., Aeschlimann, M., Mathias, S., and Schneider, C. M., "Spin-resolved photoelectron spectroscopy using femtosecond extreme ultraviolet light pulses from high-order harmonic generation," *Review of Scientific Instruments* **87**(4) (2016).

[7] Hellmann, S., Rossnagel, K., Marczynski-Bühlow, M., and Kipp, L., "Vacuum space-charge effects in solid-state photoemission," *Phys. Rev. B* **79**, 035402 (Jan 2009).

[8] Maklar, J., Dong, S., Beaulieu, S., Pincelli, T., Dendzik, M., Windsor, Y. W., Xian, R. P., Wolf, M., Ernstorfer, R., and Rettig, L., "A quantitative comparison of time-of-flight momentum microscopes and hemispherical analyzers for time- and angle-resolved photoemission spectroscopy experiments," *Review of Scientific Instruments* **91**(12), 123112 (2020).

[9] Chernov, S., Bakalis, J., Kunin, A., Withers, Z. H., White, M. G., Schönhense, G., and Allison, T. K., "Optimization of time of flight momentum microscopy for pump-probe experiments," in [*The 23rd International Conference on Ultrafast Phenomena*], paper W4A.41 (2022.).

[10] Schönhense, B., Medjanik, K., Fedchenko, O., Chernov, S., Ellguth, M., Vasilyev, D., Oelsner, A., Viefhaus, J., Kutnyakhov, D., Wurth, W., Elmers, H. J., and Schönhense, G., "Multidimensional photoemission spectroscopy—the space-charge limit," *New Journal of Physics* **20**, 033004 (mar 2018).

[11] Schönhense, G., Kutnyakhov, D., Pressacco, F., Heber, M., Wind, N., Agustsson, S. Y., Babenkov, S., Vasilyev, D., Fedchenko, O., Chernov, S., Rettig, L., Schönhense, B., Wenthaus, L., Brenner, G., Dziarzhytski, S., Palutke, S., Mahatha, S. K., Schirmel, N., Redlin, H., Manschwetus, B., Hartl, I., Matveyev, Y., Gloskovskii, A., Schlueter, C., Shokeen, V., Duerr, H., Allison, T. K., Beye, M., Rossnagel, K., Elmers, H. J., and Medjanik, K., "Suppression of the vacuum space-charge effect in fs-photoemission by a retarding electrostatic front lens," *Review of Scientific Instruments* **92**, 053703 (05 2021).

[12] Eich, S., Plötzing, M., Rollinger, M., Emmerich, S., Adam, R., Chen, C., Kapteyn, H. C., Murnane, M. M., Plucinski, L., Steil, D., Stadtmüller, B., Cinchetti, M., Aeschlimann, M., Schneider, C. M., and Mathias, S., "Band structure evolution during the ultrafast ferromagnetic-paramagnetic phase transition in cobalt," *Science Advances* **3**(3) (2017).

[13] Nicholson, C. W., Lücke, A., Schmidt, W. G., Puppin, M., Rettig, L., Ernstorfer, R., and Wolf, M., "Beyond the molecular movie: Dynamics of bands and bonds during a photoinduced phase transition," *Science* **362**(6416), 821–825 (2018).

[14] Kumar, N., Cui, Q., Ceballos, F., He, D., Wang, Y., and Zhao, H., "Exciton-exciton annihilation in mose$_2$ monolayers," *Phys. Rev. B* **89**, 125427 (Mar 2014).

[15] Hädrich, S., Rothhardt, J., Krebs, M., Demmler, S., Klenke, A., Tünnermann, A., and Limpert, J., "Single-pass high harmonic generation at high repetition rate and photon flux," *Journal of Physics B: Atomic, Molecular and Optical Physics* **49**(17), 172002 (2016).

[16] Madeo, J., Man, M. K. L., Sahoo, C., Campbell, M., Pareek, V., Wong, E. L., Al-Mahboob, A., Chan, N. S., Karmakar, A., Mariserla, B. M. K., Li, X., Heinz, T. F., Cao, T., and Dani, K. M., "Directly visualizing the momentum-forbidden dark excitons and their dynamics in atomically thin semiconductors," *Science* **370**(6521), 1199–1204 (2020).

[17] Puppin, M., Deng, Y., Nicholson, C. W., Feldl, J., Schröter, N. B. M., Vita, H., Kirchmann, P. S., Monney, C., Rettig, L., Wolf, M., and Ernstorfer, R., "Time- and angle-resolved photoemission spectroscopy of solids in the extreme ultraviolet at 500 khz repetition rate," *Review of Scientific Instruments* **90**, 023104 (2019/07/28 2019).

[18] Keunecke, M., Möller, C., Schmitt, D., Nolte, H., Jansen, G. S. M., Reutzel, M., Gutberlet, M., Halasi, G., Steil, D., Steil, S., and Mathias, S., "Time-resolved momentum microscopy with a 1 mhz high-harmonic extreme ultraviolet beamline," *Review of Scientific Instruments* **91**(6), 063905 (2020).

[19] Mills, A. K., Zhdanovich, S., Na, M. X., Boschini, F., Razzoli, E., Michiardi, M., Sheyerman, A., Schneider, M., Hammond, T. J., Süss, V., Felser, C., Damascelli, A., and Jones, D. J., "Cavity-enhanced high harmonic generation for extreme ultraviolet time- and angle-resolved photoemission spectroscopy," *Review of Scientific Instruments* **90**(8), 083001 (2019).

[20] Mills, A. K., Hammond, T. J., Lam, M. H. C., and Jones, D. J., "XUV frequency combs via femtosecond enhancement cavities," *J. Phys. B: At., Mol. Opt. Phys.* **45**(14), 142001 (2012).

[21] Pupeza, I., Zhang, C., Högner, M., and Ye, J., "Extreme-ultraviolet frequency combs for precision metrology and attosecond science," *Nature Photonics* **15**, 175–186 (2021).

[22] Medjanik, K., Fedchenko, O., Chernov, S., Kutnyakhov, D., Ellguth, M., Oelsner, A., Schonhense, B., Peixoto, T. R. F., Lutz, P., Min, C. H., Reinert, F., Daster, S., Acremann, Y., Viefhaus, J., Wurth, W., Elmers, H. J., and Schonhense, G., "Direct 3d mapping of the fermi surface and fermi velocity," *Nat Mater* **16**, 615–621 (06 2017).

[23] Chernov, S., Medjanik, K., Tusche, C., Kutnyakhov, D., Nepijko, S., Oelsner, A., Braun, J., Minár, J., Borek, S., Ebert, H., Elmers, H., Kirschner, J., and Schönhense, G., "Anomalous d-like surface resonances on mo(110) analyzed by time-of-flight momentum microscopy," *Ultramicroscopy* **159**, 453–463 (2015). Special Issue: LEEM-PEEM 9.

[24] Kunin, A., Chernov, S., Bakalis, J., Li, Z., Cheng, S., Withers, Z. H., White, M. G., Schönhense, G., Du, X., Kawakami, R. K., and Allison, T. K., "Momentum-resolved exciton coupling and valley polarization dynamics in monolayer ws$_2$," *Phys. Rev. Lett.* **130**, 046202 (Jan 2023).

[25] Li, X., Reber, M. A. R., Corder, C., Chen, Y., Zhao, P., and Allison, T. K., "High-Power Ultrafast Yb:fiber Laser Frequency Combs Using Commercially Available Components and Basic Fiber Tools," *Rev. Sci. Instrum.* **87**(9), 093114 (2016).

[26] Foltynowicz, A., Masłowski, P., Fleisher, A. J., Bjork, B. J., and Ye, J., "Cavity-enhanced optical frequency comb spectroscopy in the mid-infrared application to trace detection of hydrogen peroxide," **110**(2), 163–175 (2013).

[27] Corder, C., Zhao, P., Bakalis, J., Li, X., Kershis, M. D., Muraca, A. R., White, M. G., and Allison, T. K., "Development of a tunable high repetition rate xuv source for time-resolved photoemission studies of ultrafast dynamics at surfaces," *Proc.SPIE* **10519**, 10519 – 10519 – 7 (2018).

[28] Frassetto, F., Cacho, C., Froud, C. A., Turcu, I. E., Villoresi, P., Bryan, W. A., Springate, E., and Poletto, L., "Single-grating monochromator for extreme-ultraviolet ultrashort pulses," *Opt. Express* **19**, 19169–19181 (Sep 2011).

[29] Xiao, D., Yao, W., and Niu, Q., "Valley-Contrasting Physics in Graphene: Magnetic Moment and Topological Transport," *Phys. Rev. Lett.* **99**(23), 236809 (2007).

[30] Yao, W., Xiao, D., and Niu, Q., "Valley-Dependent Optoelectronics From Inversion Symmetry Breaking," *Phys. Rev. B* **77**(23), 235406 (2008).

[31] Cao, T., Wang, G., Han, W., Ye, H., Zhu, C., Shi, J., Niu, Q., Tan, P., Wang, E., Liu, B., and Feng, J., "Valley-Selective Circular Dichroism of Monolayer Molybdenum Disulphide," *Nat. Commun.* **3**(1), 887 (2012).

[32] Xiao, D., Liu, G.-B., Feng, W., Xu, X., and Yao, W., "Coupled Spin and Valley Physics in Monolayers of MoS_2 and Other Group-VI Dichalcogenides," *Phys. Rev. Lett.* **108**(19), 196802 (2012).

[33] Mak, K. F., He, K., Shan, J., and Heinz, T. F., "Control of Valley Polarization in Monolayer MoS_2 by Optical Helicity," *Nat. Nanotechnol.* **7**(8), 494–498 (2012).

[34] Zeng, H., Dai, J., Yao, W., Xiao, D., and Cui, X., "Valley Polarization in MoS_2 Monolayers by Optical Pumping," *Nat. Nanotechnol.* **7**(8), 490–493 (2012).

[35] Kioseoglou, G., Hanbicki, A. T., Currie, M., Friedman, A. L., Gunlycke, D., and Jonker, B. T., "Valley Polarization and Intervalley Scattering in Monolayer MoS_2," *Appl. Phys. Lett.* **101**(22), 221907 (2012).

[36] Wang, G., Chernikov, A., Glazov, M. M., Heinz, T. F., Marie, X., Amand, T., and Urbaszek, B., "Colloquium: Excitons in Atomically Thin Transition Metal Dichalcogenides," *Rev. Mod. Phys.* **90**(2), 021001 (2018).

[37] Sallen, G., Bouet, L., Marie, X., Wang, G., Zhu, C. R., Han, W. P., Lu, Y., Tan, P. H., Amand, T., Liu, B. L., and Urbaszek, B., "Robust Optical Emission Polarization in MoS_2 Monolayers Through Selective Valley Excitation," *Phys. Rev. B* **86**(8), 081301(R) (2012).

[38] Liu, G.-B., Shan, W.-Y., Yao, Y., Yao, W., and Xiao, D., "Three-Band Tight-Binding Model for Monolayers of Group-VIB Transition Metal Dichalcogenides," *Phys. Rev. B* **88**(8), 085433 (2013).

[39] Jones, A. M., Yu, H., Ghimire, N. J., Wu, S., Aivazian, G., Ross, J. S., Zhao, B., Yan, J., Mandrus, D. G., Xiao, D., Yao, W., and Xu, X., "Optical Generation of Excitonic Valley Coherence in Monolayer WSe_2," *Nat. Nanotechnol.* **8**(9), 634–638 (2013).

[40] Qiu, D. Y., da Jornada, F. H., and Louie, S. G., "Optical Spectrum of MoS_2: Many-Body Effects and Diversity of Exciton States," *Phys. Rev. Lett.* **111**(21), 216805 (2013).

[41] Xu, X., Yao, W., Xiao, D., and Heinz, T. F., "Spin and Pseudospins in Layered Transition Metal Dichalcogenides," *Nat. Phys.* **10**(5), 343–350 (2014).

[42] Glazov, M. M., Ivchenko, E. L., Wang, G., Amand, T., Marie, X., Urbaszek, B., and Liu, B. L., "Spin and Valley Dynamics of Excitons in Transition Metal Dichalcogenide Monolayers," *Phys. Status Solidi B* **252**(11), 2349–2362 (2015).

[43] Koperski, M., Molas, M. R., Arora, A., Nogajewski, K., Slobodeniuk, A. O., Faugeras, C., and Potemski, M., "Optical Properties of Atomically Thin Transition Metal Dichalcogenides: Observations and Puzzles," *Nanophotonics* **6**(6), 1289–1308 (2017).

[44] Li, H.-K., Fong, K. Y., Zhu, H., Li, Q., Wang, S., Yang, S., Wang, Y., and Zhang, X., "Valley Optomechanics in a Monolayer Semiconductor," *Nat. Photonics* **13**(6), 397–401 (2019).

[45] Zhu, B., Zeng, H., Dai, J., Gong, Z., and Cui, X., "Anomalously Robust Valley Polarization and Valley Coherence in Bilayer WS_2," *Proc. Natl. Acad. Sci. U.S.A.* **111**(32), 11606–11611 (2014).

[46] Wang, G., Bouet, L., Lagarde, D., Vidal, M., Balocchi, A., Amand, T., Marie, X., and Urbaszek, B., "Valley Dynamics Probed through Charged and Neutral Exciton Emission in monolayer WSe_2," *Phys. Rev. B* **90**(7), 075413 (2014).

[47] Lagarde, D., Bouet, L., Marie, X., Zhu, C. R., Liu, B. L., Amand, T., Tan, P. H., and Urbaszek, B., "Carrier and Polarization Dynamics in Monolayer MoS_2," *Phys. Rev. Lett.* **112**(4), 047401 (2014).

[48] Yan, T., Qiao, X., Tan, P., and Zhang, X., "Valley Depolarization in Monolayer WSe_2," *Sci. Rep.* **5**(1), 15625 (2015).

[49] Mai, C., Semenov, Y. G., Barrette, A., Yu, Y., Jin, Z., Cao, L., Kim, K. W., and Gundogdu, K., "Exciton Valley Relaxation in a Single Layer of WS_2 Measured by Ultrafast Spectroscopy," *Phys. Rev. B* **90**(4), 041414(R) (2014).

[50] Schmidt, R., Berghäuser, G., Schneider, R., Selig, M., Tonndorf, P., Malić, E., Knorr, A., de Vasconcellos, S. M., and Bratschitsch, R., "Ultrafast Coulomb-Induced Intervalley Coupling in Atomically Thin WS_2," *Nano Lett.* **16**(5), 2945–2950 (2016).

[51] Zhu, C. R., Zhang, K., Glazov, M., Urbaszek, B., Amand, T., Ji, Z. W., Liu, B. L., and Marie, X., "Exciton Valley Dynamics Probed by Kerr Rotation in WSe_2 Monolayers," *Phys. Rev. B* **90**(16), 161302(R) (2014).

[52] Dal Conte, S., Bottegoni, F., Pogna, E. A. A., De Fazio, D., Ambrogio, S., Bargigia, I., D'Andrea, C., Lombardo, A., Bruna, M., Ciccacci, F., Ferrari, A. C., Cerullo, G., and Finazzi, M., "Ultrafast Valley Relaxation Dynamics in Monolayer MoS_2 Probed by Nonequilibrium Optical Techniques," *Phys. Rev. B* **92**(23), 235425 (2015).

[53] Hsu, W.-T., Chen, Y.-L., Chen, C.-H., Liu, P.-S., Hou, T.-H., Li, L.-J., and Chang, W.-H., "Optically Initialized Robust Valley-Polarized Holes in Monolayer WSe_2," *Nat. Commun.* **6**(1), 8963 (2015).

[54] Plechinger, G., Nagler, P., Arora, A., Schmidt, R., Chernikov, A., del Águila, A. G., Christianen, P. C., Bratschitsch, R., Schüller, C., and Korn, T., "Trion Fine Structure and Coupled Spin–Valley Dynamics in Monolayer Tungsten Disulfide," *Nat. Commun.* **7**(1), 12715 (2016).

[55] Plechinger, G., Korn, T., and Lupton, J. M., "Valley-Polarized Exciton Dynamics in Exfoliated Monolayer WSe_2," *J. Phys. Chem. C* **121**(11), 6409–6413 (2017).

[56] McCormick, E. J., Newburger, M. J., Luo, Y. K., McCreary, K. M., Singh, S., Martin, I. B., Cichewicz, E. J., Jonker, B. T., and Kawakami, R. K., "Imaging Spin Dynamics in Monolayer WS_2 by Time-Resolved Kerr Rotation Microscopy," *2D Mater.* **5**(1), 011010 (2017).

[57] Schwemmer, M., Nagler, P., Hanninger, A., Schüller, C., and Korn, T., "Long-Lived Spin Polarization in n-Doped $MoSe_2$ Monolayers," *Appl. Phys. Lett.* **111**(8), 082404 (2017).

[58] Dey, P., Yang, L., Robert, C., Wang, G., Urbaszek, B., Marie, X., and Crooker, S. A., "Gate-Controlled Spin-Valley Locking of Resident Carriers in WSe_2 Monolayers," *Phys. Rev. Lett.* **119**(13), 137401 (2017).

[59] Hao, K., Moody, G., Wu, F., Dass, C. K., Xu, L., Chen, C.-H., Sun, L., Li, M.-Y., Li, L.-J., MacDonald, A. H., and Li, X., "Direct Measurement of Exciton Valley Coherence in Monolayer WSe_2," *Nat. Phys.* **12**(7), 677–682 (2016).

[60] Smallwood, C. L. and Cundiff, S. T., "Multidimensional Coherent Spectroscopy of Semiconductors," *Laser Photonics Rev.* **12**(12), 1800171 (2018).

[61] Guo, L., Wu, M., Cao, T., Monahan, D. M., Lee, Y.-H., Louie, S. G., and Fleming, G. R., "Exchange-Driven Intravalley Mixing of Excitons in Monolayer Transition Metal Dichalcogenides," *Nat. Phys.* **15**(3), 228–232 (2018).

[62] Lloyd, L. T., Wood, R. E., Mujid, F., Sohoni, S., Ji, K. L., Ting, P.-C., Higgins, J. S., Park, J., and Engel, G. S., "Sub-10 fs Intervalley Exciton Coupling in Monolayer MoS_2 Revealed by Helicity-Resolved Two-Dimensional Electronic Spectroscopy," *ACS Nano* **15**(6), 10253–10263 (2021).

[63] Purz, T. L., Martin, E. W., Rivera, P., Holtzmann, W. G., Xu, X., and Cundiff, S. T., "Coherent Exciton-Exciton Interactions and Exciton Dynamics in a $MoSe_2/WSe_2$ Heterostructure," *Phys. Rev. B* **104**(24), L241302 (2021).

[64] Mahmood, F., Alpichshev, Z., Lee, Y.-H., Kong, J., and Gedik, N., "Observation of Exciton–Exciton Interaction Mediated Valley Depolarization in Monolayer $MoSe_2$," *Nano Lett.* **18**(1), 223–228 (2017).

[65] Moody, G., Dass, C. K., Hao, K., Chen, C.-H., Li, L.-J., Singh, A., Tran, K., Clark, G., Xu, X., Berghäuser, G., Malic, E., Knorr, A., and Li, X., "Intrinsic Homogeneous Linewidth and Broadening Mechanisms of Excitons in Monolayer Transition Metal Dichalcogenides," *Nat. Commun.* **6**(1), 8315 (2015).

[66] Kioseoglou, G., Hanbicki, A. T., Currie, M., Friedman, A. L., and Jonker, B. T., "Optical Polarization and Intervalley Scattering in Single Layers of MoS_2 and $MoSe_2$," *Sci. Rep.* **6**(1), 25041 (2016).

[67] Ye, J., Li, Y., Yan, T., Zhai, G., and Zhang, X., "Ultrafast Dynamics of Spin Generation and Relaxation in Layered WSe_2," *J. Phys. Chem. Lett.* **10**(11), 2963–2970 (2019).

[68] Selig, M., Katsch, F., Brem, S., Mkrtchian, G. F., Malic, E., and Knorr, A., "Suppression of Intervalley Exchange Coupling in the Presence of Momentum-Dark States in Transition Metal Dichalcogenides," *Phys. Rev. Res.* **2**(2), 023322 (2020).

[69] Pikus, G. E. and Bir, G. L., "Exchange Interaction in Excitons in Semiconductors," *Zh. Eksp. Teor. Fiz. [Sov. Phys.—JETP]* **60**, 195–208 (1971).

[70] Yu, H., Liu, G.-B., Gong, P., Xu, X., and Yao, W., "Dirac Cones and Dirac Saddle Points of Bright Excitons in Monolayer Transition Metal Dichalcogenides," *Nat. Commun.* **5**(1), 3876 (2014).

[71] Yu, T. and Wu, M. W., "Valley Depolarization Due to Intervalley and Intravalley Electron-Hole Exchange Interactions in Monolayer MoS_2," *Phys. Rev. B* **89**(20), 205303 (2014).

[72] Glazov, M. M., Amand, T., Marie, X., Lagarde, D., Bouet, L., and Urbaszek, B., "Exciton Fine Structure and Spin Decoherence in Monolayers of Transition Metal Dichalcogenides," *Phys. Rev. B* **89**(20), 201302(R) (2014).

[73] Kormányos, A., Burkard, G., Gmitra, M., Fabian, J., Zólyomi, V., Drummond, N. D., and Falko, V., "K · P Theory for Two-Dimensional Transition Metal Dichalcogenide Semiconductors," *2D Mater.* **2**, 022001 (apr 2015).

[74] Qiu, D. Y., Cao, T., and Louie, S. G., "Nonanalyticity, Valley Quantum Phases, and Light-like Exciton Dispersion in Monolayer Transition Metal Dichalcogenides: Theory and First-Principles Calculations," *Phys. Rev. Lett.* **115**(17), 176801 (2015).

[75] Moody, G., Schaibley, J., and Xu, X., "Exciton Dynamics in Monolayer Transition Metal Dichalcogenides," *J. Opt. Soc. Am. B* **33**(7), C39 (2016).

[76] Berghäuser, G., Bernal-Villamil, I., Schmidt, R., Schneider, R., Niehues, I., Erhart, P., de Vasconcellos, S. M., Bratschitsch, R., Knorr, A., and Malic, E., "Inverted Valley Polarization in Optically Excited Transition Metal Dichalcogenides," *Nat. Commun.* **9**(1), 971 (2018).

[77] Bernal-Villamil, I., Berghäuser, G., Selig, M., Niehues, I., Schmidt, R., Schneider, R., Tonndorf, P., Erhart, P., de Vasconcellos, S. M., Bratschitsch, R., Knorr, A., and Malic, E., "Exciton Broadening and Band Renormalization Due to Dexter-Like Intervalley Coupling," *2D Mater.* **5**(2), 025011 (2018).

[78] Selig, M., Katsch, F., Schmidt, R., Michaelis de Vasconcellos, S., Bratschitsch, R., Malic, E., and Knorr, A., "Ultrafast Dynamics in Monolayer Transition Metal Dichalcogenides: Interplay of Dark Excitons, Phonons, and Intervalley Exchange," *Phys. Rev. Res.* **1**(2), 022007(R) (2019).

[79] Peng, X. and Yan, Y., "Graphene saturable absorbers applications in fiber lasers," *Journal of the European Optical Society-Rapid Publications* **17**(1), 16 (2021).

[80] Luo, Y. K., Xu, J., Zhu, T., Wu, G., McCormick, E. J., Zhan, W., Neupane, M. R., and Kawakami, R. K., "Opto-valleytronic spin injection in monolayer mos2/few-layer graphene hybrid spin valves," *Nano Letters* **17**, 3877–3883 (06 2017).

[81] Malic, E., Winzer, T., Bobkin, E., and Knorr, A., "Microscopic theory of absorption and ultrafast many-particle kinetics in graphene," *Phys. Rev. B* **84**, 205406 (Nov 2011).

[82] Mittendorff, M., Winzer, T., Malic, E., Knorr, A., Berger, C., de Heer, W. A., Schneider, H., Helm, M., and Winnerl, S., "Anisotropy of excitation and relaxation of photogenerated charge carriers in graphene," *Nano Letters* **14**, 1504–1507 (03 2014).

[83] Trushin, M., Grupp, A., Soavi, G., Budweg, A., De Fazio, D., Sassi, U., Lombardo, A., Ferrari, A. C., Belzig, W., Leitenstorfer, A., and Brida, D., "Ultrafast pseudospin dynamics in graphene," *Phys. Rev. B* **92**, 165429 (Oct 2015).

[84] Danz, T., Neff, A., Gaida, J. H., Bormann, R., Ropers, C., and Schäfer, S., "Ultrafast sublattice pseudospin relaxation in graphene probed by polarization-resolved photoluminescence," *Phys. Rev. B* **95**, 241412 (Jun 2017).

[85] Beyer, H., Hein, P., Rossnagel, K., and Bauer, M., "Ultrafast decay of carrier momentum anisotropy in graphite," *Phys. Rev. B* **107**, 115136 (Mar 2023).

[86] Aeschlimann, S., Krause, R., Chávez-Cervantes, M., Bromberger, H., Jago, R., Malić, E., Al-Temimy, A., Coletti, C., Cavalleri, A., and Gierz, I., "Ultrafast momentum imaging of pseudospin-flip excitations in graphene," *Phys. Rev. B* **96**, 020301 (Jul 2017).

[87] Winzer, T. and Malic, E., "The impact of pump fluence on carrier relaxation dynamics in optically excited graphene," *Journal of Physics: Condensed Matter* **25**, 054201 (jan 2013).

[88] Shirley, E. L., Terminello, L. J., Santoni, A., and Himpsel, F. J., "Brillouin-zone-selection effects in graphite photoelectron angular distributions," *Phys. Rev. B* **51**, 13614–13622 (May 1995).

[89] Bakalis, J., Chernov, S., Kunin, A., Chen, S., Li, Z., Corder, C., Zhao, P., Du, X., Sch'onhense, G., Kawakami, R., White, M., and Allison, T., "Direct imaging of ultrafast pseudospin relaxation in graphene probed with time-resolved momentum microscopy," *in preparation* (2024).

[90] Zhang, L., Zhang, Z., Wu, F., Wang, D., Gogna, R., Hou, S., Watanabe, K., Taniguchi, T., Kulkarni, K., Kuo, T., Forrest, S. R., and Deng, H., "Twist-angle dependence of moiréexcitons in ws2/mose2 heterobilayers," *Nature Communications* **11**(1), 5888 (2020).

[91] Alexeev, E. M., Ruiz-Tijerina, D. A., Danovich, M., Hamer, M. J., Terry, D. J., Nayak, P. K., Ahn, S., Pak, S., Lee, J., Sohn, J. I., Molas, M. R., Koperski, M., Watanabe, K., Taniguchi, T., Novoselov, K. S., Gorbachev, R. V., Shin, H. S., Fal'ko, V. I., and Tartakovskii, A. I., "Resonantly hybridized excitons in moirésuperlattices in van der waals heterostructures," *Nature* **567**(7746), 81–86 (2019).

[92] Schmitt, D., Bange, J. P., Bennecke, W., AlMutairi, A., Meneghini, G., Watanabe, K., Taniguchi, T., Steil, D., Luke, D. R., Weitz, R. T., Steil, S., Jansen, G. S. M., Brem, S., Malic, E., Hofmann, S., Reutzel, M., and Mathias, S., "Formation of moiré interlayer excitons in space and time," *Nature* **608**(7923), 499–503 (2022).

[93] Wallauer, R., Raths, M., Stallberg, K., Münster, L., Brandstetter, D., Yang, X., Güdde, J., Puschnig, P., Soubatch, S., Kumpf, C., Bocquet, F. C., Tautz, F. S., and Höfer, U., "Tracing Orbital Images on Ultrafast Time Scales," *Science* **371**(6533), 1056–1059 (2021).

[94] Neef, A., Beaulieu, S., Hammer, S., Dong, S., Maklar, J., Pincelli, T., Xian, R. P., Wolf, M., Rettig, L., Pflaum, J., and Ernstorfer, R., "Orbital-resolved observation of singlet fission," *Nature* **616**(7956), 275–279 (2023).